Accepted Manuscript

Improved performance of the rechargeable hybrid aqueous battery at near full state-of-charge

Wenlong Xiong, Dongjie Yang, Jian Zhi, Tuan K.A. Hoang, Xueqing Qiu, P. Chen

PII: S0013-4686(18)30669-8

DOI: 10.1016/j.electacta.2018.03.152

Reference: EA 31518

To appear in: *Electrochimica Acta*

Received Date: 15 January 2018

Revised Date: 23 March 2018

Accepted Date: 24 March 2018

Please cite this article as: W. Xiong, D. Yang, J. Zhi, T.K.A. Hoang, X. Qiu, P. Chen, Improved performance of the rechargeable hybrid aqueous battery at near full state-of-charge, *Electrochimica Acta* (2018), doi: 10.1016/j.electacta.2018.03.152.

Improved performance of the rechargeable hybrid aqueous battery at near full state-of-charge

Wenlong Xiong[a,b,c†], Dongjie Yang[a,c†], Jian Zhi[b], Tuan K. A. Hoang[b], Xueqing Qiu[a,c,**], P. Chen[b,*]

[a] *School of Chemistry and Chemical Engineering, South China University of Technology, Guangzhou 510640, China*

[b] *Department of Chemical Engineering and Waterloo Institute of Nanotechnology, University of Waterloo, 200 University Avenue West, Waterloo, Ontario N2L3G1, Canada*

[c] *Guangdong Engineering Research Center for Green Fine Chemicals, South China University of Technology, Guangzhou 510640, China*

[†] These authors equally contributed to this work.

***Corresponding Author**

P. Chen

E-mail: p4chen@uwaterloo.ca. Tel.: +1-519-888-4567 ext. 35586. Fax: +1-519-888-4347.

****Corresponding Author**

Xueqing Qiu

E-mail: xueqingqiu66@163.com. Tel.: +86-20-8711-4722. Fax: +86-20-8711-4721.

Abstract: For the first time, a green lignin/silica nanocomposite (LSC) is introduced to the rechargeable hybrid aqueous Zn/$LiMn_2O_4$ battery (ReHAB) as additive in the cathode formulation. Lignin acts as a key role to regulate and control the structure of LSC, intending to enhance the stability of the ReHAB by improving the float charge performance while maintaining other electrochemical performances of the battery. The lignin/silica nanocomposites (LSCs) are characterized by X-ray diffraction, scanning electron microscopy, surface area and porosimetry analyzer, and transmission electron microscopy. The results show that amorphous, uniform and mesoporous LSC-1 is prepared at the mass ratio of 1:2 of lignin to silica. LSC-1 used as the cathode additive improves the float charge performance of ReHAB via decreasing the float charge capacity by 57%. To compensate the loss of conductivity caused by LSC-1 and increase the capacity of the battery, graphene (G) is added. Compared to the reference battery, battery using the cathode containing 3 wt% combined additive of LSC-1 and G at mass ratio of 1:1, has 50% lower float charge capacity, higher rate performance and better cyclability. Up to a discharge capacity of 95 $mAh \cdot g^{-1}$ is still obtained after 300 cycles of 100% depth-of-discharge.

Keywords: lignin/silica nanocomposite; graphene; hybrid aqueous batteries; float charge capacity.

1. Introduction

Aqueous rechargeable lithium ion batteries (ARLB) are promising alternative energy storage systems to store electricity generated from renewable and clean energy resources (e.g., solar, wind, and biomass energy), partly because ARLB can overcome some disadvantages of lithium ion batteries, *i.e.*, the high cost and safety problems, and environment pollution problem of commercially aqueous Pb-acid or Ni–Cd batteries, *i.e.*, the heavy metal pollution and corrosion of strong acid and alkaline electrolyte [1–4]. The $LiMn_2O_4$ based ARLB, one typical aqueous batteries, is born in 1994 [5] and has been proven that it can function at good rate capability and cyclability [1–4,6,7]. A rechargeable hybrid aqueous battery (ReHAB), using commercial $LiMn_2O_4$ as the active material in the cathode, zinc as the anode, and an aqueous solution containing Li^+ and Zn^{2+} as the electrolyte, has been being developed by our group [8]. Importance of the ReHAB is attributed to its environmental friendliness, inherent non-flamability, low cost, and reasonable energy density [8].

To apply this low cost ReHAB as power storage (e.g. interface with grid to regulate and store electricicity from wind mill) or as uninterruptible power supply (UPS), the energy spent to maintain the battery at it 100% charged state should be as small as possible. The process applying a small current to maintain battery at fully charged state is called float charge. Low float charge current or low float charge capacity are the most beneficial criterion for electricity stores. Extensive efforts have been made continuously to improve the performances of the ReHAB to promote the progress of its commercialization. These efforts focus on the chemical modification of $LiMn_2O_4$

in the cathode [8,9], the modification of zinc anode via electroplating [10,11], and in particular, the physical modification of electrolytes, for example, the aqueous electrolyte with thiourea as additive [12] and a series of gel electrolytes [13–17]. In fact, the physical modification is very important because simple method is always easily scaled up. Except for the physical modification of electrolytes, the physical modification of cathode should be an approach to improve the performances of the ReHAB. Cathode modification is important in many types of rechargeable batteries. For instance, an appropriate amount of additive, silica, has significant improvement on the performances of Li-S batteries, when it is blended into the cathode [18–20]. The dissolution of Mn^{2+} derived from the decomposition of $LiMn_2O_4$ into the electrolyte appears in the ReHAB [8,21,22]. This problem cause poor float charge performance of the ReHAB. That is to say, the float charge performance of the ReHAB could be improved by slowing down the diffusion of Mn^{2+} into the electrolyte. In fact, silica, a material attracted substantial academic and industrial interest, has been proven that it can effectively adsorb Mn^{2+} [23].

Silica can be prepared by many methods, such as sol-gel, microemulsion, precipitation, or commercial fuming [24]. Comparing with the other methods, the precipitated silica may be the most appropriate candidate additive for the ReHAB because of its ease of preparation and very low cost. However, the dispersity of silica is low owing to the agglomeration caused by the luxuriant silanol (Si–OH) groups on its surface [24]. Besides the traditional approaches, which are the addition of expensive and toxic modifiers in the precipitation process, people have found out

some novel, cheap, and renewable modifiers, for example, lignin, to tackle the issue of agglomeration between precipitated silica particles by preparing the precipitated lignin/silica composite (LSC) [25–27].

Lignin, which accounts for 15–40 wt% of wood, is the second most abundant biopolymer and the largest natural renewable resource of aromatic compounds on the earth [28,29]. Despite the traditional low-valued uses of industrial lignin, the novel applications are focused on introducing industrial lignin into different high value-added areas, such as nanomaterials [30–32], UV-absorbent additives for polymers [27,33], sun blocker for sunscreens [34,35] and lignin/silica composites (LSCs) [25–27,36]. Especially, LSCs have opened up several promising application areas for lignin [37–39]. As far as we know, there are no reports referring to the use of LSCs as additives in batteries. Inspired from the successful experience of silica additive in the cathode of Li-S batteries [18–20], here we add LSC to the cathode of ReHAB for the first time.

In the present study, the uniform LSC was prepared by a simple one-pot method [27], and used as additives to modify the cathode of ReHAB. The LSC prepared at the mass ratio of 1:2 of lignin to silica was found to be able to significantly improve the float charge performance of ReHAB by decreasing the float charge capacity. However, it also dramatically decreases the discharge capacity of ReHAB due to its insulation. To compensate the loss of conductivity caused by LSC, graphene (G) is employed as a additive for the cathode of ReHAB due to its superior electronic conductivity [40–44]. Benefiting from the cooperation of LSC and G, ReHAB using the cathode

containing LSC and G as a combined additive (LSC + G) can operate at a very low float charge capacity and high discharge capacity. The capacity retention after 300 cycles at 1 C of ReHAB using the cathode cotaining LSC + G is very close to that of the battery using reference cathode and much higher than that of the battery using cathode only containing G as the additive. The float charge performance is emphatically considered in this study because the ReHAB is a promising alternative for the application of UPS. In this regard, float charge performance is the most important criterion [13].

2. Experimental

2.1 Materials

The source and pretreatment of pine alkali lignin (AL) were presented in our previous work [26]. $LiMn_2O_4$ was purchased from Shanshan Co. (Changsha, China). Graphene (G) was purchased from Tanyuan Technology Co., Ltd. (Changzhou, China). Other reagents, such as sodium metasilicate pentahydrate ($Na_2SiO_3 \cdot 5H_2O$), 60 wt% 3-chloro-2-hydroxypropyltrimethylammonium chloride (CHPTMAC) aqueous solution, ammonium chloride, lithium hydroxide, and sodium hydroxide, were of analytical grade and purchased from Sigma-Aldrich Co.. Sulfuric acid (95−98 wt%, ACS plus grade) was purchased from Fisher Scientific Co..

2.2 Synthesis of Quaternized alkali lignin (QAL)

The QAL was synthesized following the same processes presented in our previous

work [27].

2.3 Preparation of LSCs and silica

The LSCs were prepared following the same process presented in our previous work [27]. Three LSCs, named as LSC-1, LSC-2, and LSC-3, were prepared based on the different initial mass ratios of QAL to SiO_2 (QAL: SiO_2 = 0.5, 1.0, 1.5, respectively).

The preparation process of silica was almost the same as the one of LSC, except the addition process of QAL. $Na_2SiO_3 \cdot 5H_2O$ (5.3 g) was first dissolved in an ethanol-water mixture (the volume ratio of absolute ethanol to deionized water was 1:6). The mixture was stirring for 30 min at 35 ºC. Subsequently, the mixture was adjusted to a pH of 10.5 using aqueous ammonium chloride solution (2 M) and then stirred for 3 h. After that, the mixture was adjusted to a pH of 7.0 using aqueous sulfuric acid (20 wt%) and then stirred for 30 min. When the reaction came to the end, the mixture was aged for 1 h at 40 ºC. Finally, the silica was collected by suction filtration, washed several times with neutral deionized water and dried in an oven at 60 ºC.

2.4 Preparation of cathodes, anode, electrolytes, and batteries

The reference cathode was prepared by mixing $LiMn_2O_4$ (Shanshan Co.), KS-6 graphite (Imerys Graphite & Carbon), and polyvinylidene fluoride (PVdF, Kynar®, HSV900) (86:7:7 wt%) in n-methyl-2-pyrrolidone (NMP, Sigma-Aldrich Co., 99.5%

purity) for 10 min with Planetary Centrifugal Mixer (AR-100, ThinkUSA). The slurry was coated on a conductive polyethylene (PE) film (All-Spec 854-36150) and placed in 60 °C vacuum oven for 6 h. The dried slurry with substrate of PE film was cut in a disk with 12 mm diameter to be used as the cathode. The loading of cathode is 5−7 mg of $LiMn_2O_4$ per cm^2. The other cathodes with additives were prepared by mixing $LiMn_2O_4$, KS-6 graphite, PVDF (86:7:7 wt%), and different additives (LSC, G, and LSC+G) in NMP with Planetary Centrifugal Mixer, respectively. It should be note that each additive was blended with KS first, and then the mixture of additive and KS-6 was mixed with $LiMn_2O_4$ and PVDF in NMP. The dosages of the additives were determined based on the mass of $LiMn_2O_4$. The other procedures were the same as the reference one.

The zinc anode was prepared by polishing the commercial zinc foil (Rotometals, 99.6% purity) using 0.3 μm polishing powder (Boehler) dispersed in deionized water and a nanocloth (Boehler). Each side of the zinc foil was polished for 10 min. The polished zinc foil was washed with deionized water, followed by rinsing with ethanol and dried at 60 °C under vacuum for 30 min. Zinc anode was obtained by cutting from the polished zinc foil to round shape disk with diameter of 12 mm.

The electrolyte was prepared by dissolving 2 M zinc sulfate heptahydrate (Alfa Aesar Co., 98%) and 1 M lithium sulfate (Sigma-Aldrich Co., 98%) in deionized water. The pH of the solution was adjusted to 4.00 ± 0.05 using sulfuric acid or lithium hydroxide solution.

The cathode, Absorbed Glass Mat (AGM, NSG Co.) separator, electrolyte, and zinc

anode were assembled into a coin cell (CR 2025).

2.5 Characterization

LSCs and the prepared silica were characterized by a powder X-ray diffraction (XRD, D8 Discover, Brüker) instrument equipped with a Cu Kα radiation source, with a scan speed of 1° per minute, ranging from 10° to 90°, an accelerated surface area and porosimetry analyzer (ASAP2020, Micromeritics) using a 20-point nitrogen adsorption and desorption program based on the Brunauer–Emmett–Teller (BET) method, a field emission scanning electron microscopy (SEM, Merlin, Zeiss Corp., Germany) at 10 kV, and a transmission electron microscopy (TEM, LIBRA® 200 MC, Zeiss Corp., Germany).

2.6 Electrochemical measurements

The float charge performance, which was presented by the float charge capacity, was tested by an NEWARE battery tester (NEWARE Battery Test System, Neware Co. Ltd., China) at room temperature. The test program was charging the battery from 1.4 to 2.1 V (vs Zn^{2+}/Zn) by a constant current (CC) mode at 0.2 C rate (1 C is defined as 115 $mAh \cdot g^{-1}$), then charging the battery to maintain it at 2.1 V by a constant voltage (CV) mode for 24 h, and finally discharging the battery to 1.4 V by the CC mode at 0.2 C rate. The open circuit voltage (OCV) was measured following the test of float charge performance. For this purpose, the battery voltage was recorded when the battery was at resting state, e.g. not charging or discharging , and finally discharging

the battery to 1.4 V by the CC mode at 0.2 C rate.

The rate performance of the battery was tested by the NEWARE battery tester at various CC charge−CC discharge rates from 0.2 C to 4 C at room temperature.

The galvanostatic charge-discharge cycling of the batteries was carried out between 1.4 and 2.1 V, in CC−CV mode at room temperature at 1 C rate with the NEWARE battery tester. The current cutoff during CV charging was set at 10% of the charging current in the CC charging step at 1 C rate.

Cyclic voltammetry (CV) tests were conducted on a multichannel potentiostat (VMP3, Biologic) between 1.4 and 2.1 V at a scan rate of 0.1 $mV \cdot s^{-1}$. In addition, AC impedance measurements were performed with amplitude of 10 mV at the applied frequency range from 0.1 Hz to 1 MHz after the batteries were cycled for 10 cycles at 1 C rate. With the same running program, AC impedance was implemented on a three-electrode cell with the battery cathode as the working electrode (WE), platinum as the counter electrode (CE), and standard calomel electrode (SCE) as the reference electrode (RE). These data were fitted by using ZView and the Li^+ diffusion coefficient was calculated for each of the cathode (Supporting information).

3. Results and discussion

3.1 Specific surface areas, pore volume distributions, and TEM images of LSCs

The N_2 adsorption–desorption isotherms on LSCs prepared with different initial mass ratios of silica and QAL are presented Fig. 1(a). All of the samples are amorphous materials, as evidenced by the XRD results in Fig. S1 (Supporting

information). The lower portion of the loop is traced out on adsorption, and the upper portion on desorption. At low relative pressure ($P/P_0 < 0.4$), the quantity absorbed of N_2 almost accounts for half of the total adsorbed nitrogen for each material. This suggests that the materials possess some porous characteristics [13]. The hysteresis loops observed in the adsorption–desorption isotherm of all samples, which resembled type IV of Brunauer's classification [45], indicate all the samples possess mesoporous structure. The hysteresis loop in the adsorption–desorption isotherm of LSC-1 is markedly bigger than that of the other two samples, which means there are more abundant mesopores in LSC-1. When it comes to high relative pressure ($P/P_0 > 0.9$), the capillary condensation occurs in the adsorption–desorption isotherm of each sample may be owing to the small sizes of particles in the materials [46].

The pore volume curves are shown in Fig. 1(b). Obviously, the tendency of pore volume distribution and pore size of LSC-1 are different from that of the other two samples. There are some micropores (pore size less than 2 nm) that cannot be measured by the instrument in silica (Fig. S2, Supporting information), LSC-2 and LSC-3, but they are absent in LSC-1 with average pore width of 3.45 nm (Table S1, Supporting information). It indicates that the prepared LSC will be uniform mesoporous materials when the initial mass ratio of QAL and silica is 0.5:1. This is because the negatively protogenous silica crystal nucleus are easier bonded to the three-dimensional network structure of QAL by the strong interaction between the surface acidic groups of silica and the basic cationic quaternary ammonium groups in QAL, to prevent the protogenous silica crystal nucleus from aggregating into

non-porous or microporous silica by themselves. If the initial mass ratio of QAL and silica reaches 1.0:1 and 1.5:1, the self-aggregation of QAL in aqueous solution will be enhanced due to the increase of the concentration of QAL [47–49], resulting in the loss of ability to control the formation of mesoporous structures. In particular, when the initial mass ratio of QAL and silica reaches to 1.5:1, the uniform spherical morphology of the prepared LSC-3 is destroyed compared with that of silica, LSC-1 and LSC-2, as evidenced by the SEM images in Fig. S3 (Supporting information). There is some shapeless QAL coating on the surface of particles owing to the enhancement of self-aggregation of QAL, because the self-aggregation of lignin derivatives increases when the concentration increases in aqueous solution [47–49]. This is further demonstrating the self-aggregation of QAL will inhibit the formation of uniform spherical LSC with mesoporous structures.

In fact, the formation of LSC includes two steps in the one-pot method [27]. The first one is the generation of silica at pH 10.5 accompanied by the formation of pore structure and the second one is the deposition of QAL on silica to form the LSC along with the pH decreasing from 10.5 to 7. According to our results in Fig. 1, 0.5 is the opportune initial mass ratio of QAL to SiO_2 to prepare the LSC with pure mesopore. Comparing the data of LSC-1 with LSC-2 in Table S1 (Supporting information), the pore volume obviously decreases along with the increase of QAL. However, comparing the data of LSC-2 with LSC-3 in Table S1 (Supporting information), the pore volume doesn’t change too much along with the increase of QAL. This suggests that the formation of pore structure of LSC in the first step is almost the same after the

initial mass ratio of QAL to SiO_2 reaches to a certain value (≥ 1). So the pore volume of LSC is almost maintained although the initial mass ratio of QAL to SiO_2 increases from 1.0 to 1.5. In the premise of similar first step, too much QAL aggregation will affect the second step, which is reflected by the significantly decrease in BET surface area, comparing the data of LSC-2 with LSC-3 in Table S1 (Supporting information).

TEM is employed to further characterize the structure of LSCs. As shown in Fig. S4 (Supporting information), the precipitated silica is uniform and amorphous, which is consistent with the results of XRD and SEM analyses. In addition, there seems to be some irregular pores in the silica particle, as evidenced by the transmission of light of particles in Fig. S4. Compared to the structure of silica, the LSC-1 and LSC-2 are also uniform and amorphous. However, the surface of LSC-1 and LSC-2 are majorly coated with QAL, as evidenced by the obvious core-shell structure in Fig. 2. The irregular pores are also existed in the LSC-1 particles but nearly absent in the LSC-2 particles, which means too much QAL will inhibit the formation of pore structure. It is hard to distinguish the differnece between the pores in silica and LSC-1 only depended on the TEM images in Fig. S4 and Fig. 2, but the BET method and pore size distribution can distinguish it. According to the analyses of N_2 adsorption–desorption isotherms, pore size distributions, and TEM images, it can be determined that LSC-1 is the pure mesoporous material.

3.2 Float charge performances of the batteries

High float charge capacity/current is one of the major drawbacks for aqueous

lithium batteries. Thus, minimization of the float charge capacity is highly desirable while quite challenging in designing highly stable aqueous batteries. Table 1 presents the discharge capacity and float charge capacity at 0.2 C of the batteries based on the different cathodes with or without additives. The data in this table is aimed at evaluating which LSC is the best for improving the float charge performance, which is presented by the decrease of the float charge capacity of the battery. After mixing 2 wt% of silica into the cathode, the float charge capacity of the battery decreases from 14.3 to 9.4 $mAh \cdot g^{-1}$ (Table S2, Supporting information). This is a good and the decrease of the float charge capacity may be contributed by the following approach. The mesoporous silica possesses the ability to adsorb Mn^{2+} according to Yang's research [23]. There are some mesopores in the precipitated silica according to the results of N_2 adsorption–desorption isotherm and pore volume curve (Fig. S2, Supporting information). Hence, the mesopores in silica may contribute to improving the float charge performance, because the mesopores may adsorb Mn^{2+} derived from the decomposition of $LiMn_2O_4$ in the acidic electrolyte to prevent it from dissolving into the electrolyte. Meanwhile, the discharge capacity also decreases from 119.1 to 113.8 $mAh \cdot g^{-1}$ (Table S2, Supporting information), because the loss of the conductivity of the cathode inevitably results in a slight decrease of the discharge capacity.

The precipitated silica can improve the float charge performance of the cathode, but the enhancement is not very significant. The silica based composites may be an attemptable approach. Because many kinds of composites can exert multiple

advantages of the different components in the composites, and some of the advantages are even much better than a single component. Herein presents the amorphous LSC, which is prepared by a novel, simple and environmentally friendly one-pot method in an aqueous solution. This idea is evidenced to be practicable by the data presented in Table 1. After mixing 2 wt% of LSC-1 into the cathode, it shows the biggest ability to decrease the float charge capacity, which is decreased from 14.3 to 6.1 $mAh \cdot g^{-1}$, approximately 57.3% lower. If the lignin content in the LSC increases, the float charge capacity will also increase. This suggests that purely mesoporous LSC-1 possesses stronger ability to improve the float charge performance of the batteries than that of silica, LSC-2 and LSC-3 with micropores and some small size mesopores. According to Yang's research [23], the bigger the average pore size within the range of 10 nm of mesopores, the stronger the adsorption capacity of Mn^{2+}. Therefore, it can be expected that the purely mesoporous LSC-1 can adsorb more Mn^{2+} derived from the decomposition of $LiMn_2O_4$ in the mild acidic electrolyte, because there are more large mesopores within the pore size range of 10 nm in LSC-1 than that of in silica, LSC-2, and LSC-3 based on the results of pore volume curves. In addition, the cathode containing LSC-3 shows the worst float charge performance, which also may be due to the non-uniform particle morphology of LSC-3, as evidenced by the SEM images presented in the Fig. S3 (Supporting information). This indicates that the uniform morphology of LSC is also request for improving the float charge performance of the battery. According to the analyses in part 3.1, LSC-3 doesn't have the similar pore structure as that of LSC-1 to hold the Mn^{2+} and includes too much

lignin aggregates while lignin itself increases the float charge capacity (Table S2, Supporting information). Therefore, the float charge capacity of LSC-3 increases more than that of LSC-1. Because the purpose of the research is to improve the float charge performance by decreasing the float charge capacity, LSC-1 is considered as the most promising additive to achieve this goal. However, the most urgent issue of LSC-1 is that the discharge capacity of battery using the cathode containing LSC-1 decreases due to the loss of conductivity of the cathode.

In order to compensate the loss of conductivity caused by LSC-1, graphene, an excellent material with extraordinary electronic transport property, is also introduced into the cathode as a partner with LSC-1. The results of float charge performance of the battery using cathode with LSC, G (graphene) and LSC+G are presented in Table 2, respectively. The discharge capacity of battery using the cathode containing 2 wt% G increase from 119.1 to 122.1 $mAh \cdot g^{-1}$, and meanwhile, the float charge capacity decrease from 14.3 to 9.9 $mAh \cdot g^{-1}$ compared to the battery using reference cathode. As described in part 2.4 of the experimental section, the conductive carbon (KS-6) is mixed with G first, that is, part of the surface of KS-6 is modified by G. There is a published paper proving that the oxidation/consumption of KS-6 on the cathode/electrolyte interface is inhibited after the LMO cathode is coated with reduced graphene oxide [44], which helps to reduce the float charge capacity. Therefore, the oxidation/consumption of KS-6 on the cathode/electrolyte interface should be suppressed more or less because of the surface modifaction of KS-6 by G, leading to the decrease in float charge capacity. The ability of G to improve the float

charge performance is not better than that of LSC-1, but the ability of G to increase the discharge capacity is superior to that of LSC-1.

After mixing both LSC-1 and G into the cathode, there are some different results under the condition of different mass ratios of LSC-1 and G. When the cathode is blended with 2 wt% LSC-1+G at the mass ratio of 1:1, the discharge capacity increase from 110.1 to 115.5 $mAh \cdot g^{-1}$ and the float charge capacity also increase from 6.1 to 7.9 compared to that of the cathode with 2 wt% LSC-1. The discharge capacity (115.5 $mAh \cdot g^{-1}$) of battery using the cathode containing 2 wt% LSC-1+G (1:1) is still lower than that of the reference cathode (119.1 $mAh \cdot g^{-1}$), indicating that the G cannot completely compensate the loss of conductivity caused by LSC-1 at this condition. If the dosage of LSC-1+G (1:1) increases to 3 wt%, the discharge capacity reaches to 122.1 $mAh \cdot g^{-1}$ and the float charge capacity just slightly increase to 7.2 $mAh \cdot g^{-1}$ compared to that of the cathode containing 2 wt% LSC-1. It indicates that battery using the cathode containing 3 wt% LSC-1+G (1:1) possesses higher discharge capacity and much lower float charge capacity than that of the battery using reference cathode. Especially the float charge capacity is reduced by approximately 50%, which is an exciting result. If the dosage of LSC-1+G (1:1) in the cathode continuously increase to 4 wt%, the discharge capacity will further go up to 124.7 $mAh \cdot g^{-1}$, but the float charge capacity will also dramatically go up to 12.4 $mAh \cdot g^{-1}$ compared to that of battery using the cathode containing 3 wt% LSC-1+G (1:1). These results suggest that LSC-1 and G can play a synergistic interaction to slightly increase the discharge capacity and significantly decrease the float charge capacity at an appropriate

formula.

When the total dosage of LSC-1 and G in the cathode is fixed at 4 wt%, the float charge performance is not as good as that of the cathode containing 3 wt% LSC-1+G (1:1), although the mass ratio of LSC-1 to G changes from 1:1 to 2:1. In order to clearly show the float charge performance, an assistant parameter FC/DC, the value of dividing the discharge capacity by the float charge capacity, is artificially defined to represent the float charge performance only when the discharge capacity is higher than the reference one or at least closed to the reference one. The lower the FC/DC is, the better the float charge performance is. The FC/DC of battery using the reference cathode, the cathode containing 2 wt% G, 3 wt% LSC-1+G (1:1), 4 wt% LSC-1+G (1:1), and 4 wt% LSC-1+G (1.5:1) is 12.0%, 8.1%, 5.9%, 9.9%, and 8.6%, respectively. Obviously the float charge performance of the battery using cathode containing 3 wt% LSC-1+G (1:1) is the best.

3.3 Rate capabilities of the batteries

Fig. 3 presents the rate performance of the batteries assembled by the reference cathode, cathode containing 2 wt% LSC-1, cathode containing 2 wt %G, and the different LSC-1+G based cathodes, respectively. After the cathode is mixed with 2 wt% LSC-1, the discharge capacities are sharply decreased at each rate compared to the reference cathode, which means LSC-1 can dramatically decrease the rate performance of the battery. The battery using cathode containing 2 wt% G can maintain the discharge capacities at 0.5 C, 1 C and 2 C, slightly increase the discharge

capacity at 0.2 C, and obviously increase the discharge capacity at 4 C compared to the battery using reference cathode, which means G can improve the rate performance of the battery. The battery using cathode containing 3 wt% LSC-1+G (1:1) has the similar trend on the rate performance, maintaining the discharge capacities at 0.5 C, 1 C and 2 C and slightly increasing the discharge capacities at 0.2 C and 4 C compared to the battery using reference cathode. Subsequently the rate performances are not obviously promoted when the dosage or mass ratio of LSC-1 and G changes. Hence, among the cathodes using LSC-1 and G as the additives together, the cathode containing 3 wt% LSC-1+G (1:1) is considered as the best and selected to evaluate the cycle performance according to the analyses of float charge performance and rate performance.

3.4 Cyclabilities of the batteries

Fig. 4 presents constant current−constant voltage (CC−CV) cycling performances of batteries at 1 C for up to 300 cycles. Capacity fading is observed on all batteries owing to unwanted side reactions, including the manganese dissolution, water decomposition, hydrogen evolution, and Zn corrosion [13,21,22,50]. The discharge capacity of battery using the cathode containing 2 wt% LSC-1 on the first cycle is 104.5 $mAh \cdot g^{-1}$, which is much lower than the 114.7 $mAh \cdot g^{-1}$ of the battery using reference cathode. The discharge capacity of battery using the cathode containing 2 wt% G on the first cycle is 120.8 $mAh \cdot g^{-1}$, which is much higher than that of the battery using reference cathode. The discharge capacity of battery using the cathode

containing 3 wt% LSC-1+G (1:1) is 122.3 $mAh \cdot g^{-1}$ on the first cycle, which is also much higher than that of the battery using reference cathode. This suggests that the LSC-1 and G combined additives can perform the ability of G to increase the capacity of the battery owing to the successful compensation on the loss of conductivity of the cathode caused by LSC-1. After 300 cycles the discharge capacity of battery using the cathode containing 3 wt% LSC-1+G (1:1) is 94.3 $mAh \cdot g^{-1}$, which is still higher than the 91.3 $mAh \cdot g^{-1}$ of the battery using reference cathode. For the battery using cathode containing 2 wt% G, the most serious issue is that the capacity retention is lower than that of the reference battery, that is to say, the discharge capacity will decrease faster than that of the reference one. This issue can almost be fixed by LSC-1, which can increase the capacity retention of the battery for up to 250 cycles. The final capacity retention of the battery using cathode containing 3 wt% LSC-1+G (1:1) is 77.0%, which is very close to the 79.6% of the battery using reference cathode and much higher than the 70.8% of the battery using cathode containing 2 wt% G. Hence, the battery using the cathode containing 3 wt% LSC-1+G (1:1) can inherit the ability to increase the discharge capacity of G and the ability to maintain the capacity retention of LSC-1, leading to a higher discharge capacity than the reference one for up to 300 cycles at 1 C.

3.5 OCV, PEIS and CV of the batteries

Fig. 5 presents the open circuit voltages (OCV) versus time of the fully charged coin cells using reference cathode, cathode containing LSC-1, G, and LSC-1+G,

respectively. OCV of 1966.4 mV is observed for the battery using cathode containing 2 wt% LSC-1 after 24 h monitoring. The OCV value is much lower than that of the reference ones at 1979.8 mV. This disadvantage of LSC-1 is nearly fixed by G, as evidenced by the result that the OCV of 1977.1 mV is observed for the battery using cathode containing 3 wt% LSC-1+G (1:1) after 24 h monitoring, which is very close to that of the reference ones at 1979.8 mV.

Potential static impedance spectroscopy (PEIS) results from three-electrode-cell (WE: the cathode of the battery, CE: Pt, RE: SCE) are presented in Fig. 6. The Li^+ diffusivity can be calculated based on the PEIS data [44] and the relative fitting results are shown in Table 3. They correlate well with the battery performance. The cathode with 2 wt% LSC-1 has slightly higher Ohmic and charge transfer resistances because LSC-1 is insulating. Furthermore, the Li^+ diffusivity decreases by *ca*. 21%. This slow diffusion limits the battery performance at high rate capability and decreases the initial discharge capacity at 4 C. When adding graphene into the electrode, the Li^+ diffusivity is enhanced by a large margin of 75% and the charge transferred resistance decreases by nearly half. This explains the improved performance in rate, specific discharge capacity. However, the float charge capacity increases compared with that of LSC-1. A balance between graphene and LSC-1 (3 wt% of LSC-1 : G = 1 : 1) would solve the problem nicely. The rate capability and specific discharge capacity are improved while the float charge capacity is kept at low level.

The cyclic voltammetry (CV) results of battery using the reference cathode and the cathode containing 3 wt% LSC-1+G (1:1) are shown in Fig. S5 (Supporting

information), respectively. All currents at 1C rate are normalized to the electrode loadings. In the CV results, the two steps of intercalation/extraction of Li^+ into/out of the $LiMn_2O_4$ lattice are presented by the two distinctive pairs of reduction/oxidation peaks. It is observed that there is slight increase in the current of the battery using cathode containing 3 wt% LSC-1+G (1:1) compared to that of the reference battery, suggesting that the internal resistance and kinetics of electrochemical reactions in the batteries are slightly altered. This is expected because G improves the conductivity of the cathode owing to its excellent electrochemical activity, although LSC-1 is electrochemically inert under the testing conditions and in the voltage window of 1.4−2.1 V vs. Zn^{2+}/Zn. Meanwhile, the potentials vs. Zn^{2+}/Zn of different cathodes are almost the same. This indicates that different types of cathodes exert similar electrochemistry impacts on the intercalation and deintercalation of Li^+ into and out of the cathode. That is to say, 3 wt% LSC-1+G (1:1) just slightly enhances the speed rather than changes the approach of the intercalation and extraction of Li^+ into and out of the cathode.

4. Conclusions

In this work, the performance of the ReHAB was optimized by a new formulation of the cathode containing a combined additive of lignin/silica composite (LSC) and graphene (G). After mixing 3 wt% of LSC-1+G (1:1) into the cathode, the overall performance of the battery is superior to that of the reference battery as evidenced by the following details. The float charge capacity decreases from 14.3 to 7.2 $mAh \cdot g^{-1}$,

which is accounted for a decrease of 49.7%. The rate performance is improved as evidenced by the increase of discharge capacity at 0.2 C and 4 C and the maintenance of discharge capacity at 0.5 C, 1 C, and 2 C. For the cycling performance, the initial discharge capacity increases from 114.7 to 122.3 $mAh \cdot g^{-1}$ and the discharge capacity after 300 cycles is still higher than that of the battery using reference cathode. This study demonstrates that the performance of ReHAB can be greatly improved through cathode formulation, meanwhile, contributes to promoting the progress in research of high value-added application of renewable lignin resources.

Acknowledgements

This research is financially supported by the National Natural Science Foundation of China (No. 21436004), Natural Science Foundation of Guangdong Province (2017A030308012), Positec Canada Ltd., and Chinese Scholarship Council (CSC).

References

[1] Y.G. Wang, J. Yi, Y.Y. Xia, Recent progress in aqueous lithium-ion batteries, Adv. Energy Mater. 2 (2012) 830.

[2] W. Tang, Y.S. Zhu, Y.Y. Hou, L.L. Liu, Y.P. Wu, K.P. Loh, H.P. Zhang, K. Zhu, Aqueous rechargeable lithium batteries as an energy storage system of superfast charging, Energy Environ. Sci. 6 (2013) 2093.

[3] H. Kim, J. Hong, K.-Y. Park, H. Kim, S.-W. Kim, K. Kang, Aqueous rechargeable

Li and Na ion batteries, Chem. Rev. 114 (2014) 11788.

[4] N. Alias, A.A. Mohamad, Advances of aqueous rechargeable lithium-ion battery: a review, J. Power Sources 274 (2015) 237.

[5] W. Li, J.R. Dahn, D.S. Wainwright, Rechargeable lithium batteries with aqueous electrolytes, Science 264 (1994) 1115.

[6] L. Tian, A.B. Yuan, Electrochemical performance of nanostructured spinel $LiMn_2O_4$ in different aqueous electrolytes, J. Power Sources 192 (2009) 693.

[7] H. Manjunatha, G.S. Suresh, T.V. Venkatesha, Electrode materials for aqueous rechargeable lithium batteries, J. Solid State Electrochem. 15 (2011) 431.

[8] J. Yan, J. Wang, H. Liu, Z. Bakenov, D. Gosselink, P. Chen, Rechargeable hybrid aqueous batteries, J. Power Sources 216 (2012) 222.

[9] G.H. Yuan, J.T. Bai, T.N.L. Doan, P. Chen, Synthesis and electrochemical investigation of nanosized $LiMn_2O_4$ as cathode material for rechargeable hybrid aqueous batteries, Mater. Lett. 137 (2014) 311.

[10] K.E.K. Sun, T.K.A. Hoang, T.N.L. Doan, Y. Yu, X. Zhu, Y. Tian, P. Chen, Suppression of dendrite formation and corrosion on zinc anode of secondary aqueous batteries, ACS Appl. Mater. Interfaces 9 (2017) 9681.

[11] K.E.K. Sun, T.K.A. Hoang, T.N.L. Doan, Y. Yu, P. Chen, Highly sustainable zinc anodes for a rechargeable hybrid aqueous battery, Chem. Eur. J. 23 (2017). DOI: 10.1002/chem.201704440

[12] X.W. Wu, Y.H. Li, C.C. Li, Z.X. He, Y.H. Xiang, L.Z. Xiong, D. Chen, Y. Yu, K. Sun, Z.Q. He, P. Chen, The electrochemical performance improvement of

$LiMn_2O_4$/Zn based on zinc foil as the current collector and thiourea as an electrolyte additive, J. Power Sources 300 (2015) 453.

[13] C.Y. Lu, T.K.A. Hoang, T.N.L. Doan, H.B. Zhao, R. Pan, L. Yang, W.S. Guan, P. Chen, Rechargeable hybrid aqueous batteries using silica nanoparticle doped aqueous electrolytes, Appl. Energy 170 (2016) 58.

[14] C.Y. Lu, T.K.A. Hoang, T.N.L. Doan, M. Acton, H.B. Zhao, W.S. Guan, P. Chen, Influence of different silica gelling agents on the performance of aqueous gel electrolytes, J. Ind. Eng. Chem. 42 (2016) 101.

[15] T.K.A. Hoang, T.N.L. Doan, C.Y. Lu, M. Ghaznavi, H.B. Zhao, P. Chen, Performance of thixotropic gel electrolytes in the rechargeable aqueous Zn/$LiMn_2O_4$ battery, ACS Sustainable Chem. Eng. 5 (2017) 1804.

[16] T.K.A. Hoang, M. Acton, H.T.H. Chen, Y. Huang, T.N.L. Doan, P. Chen, Sustainable gel electrolyte containing Pb^{2+} as corrosion inhibitor and dendrite suppressor for the zinc anode in the rechargeable hybrid aqueous battery, Mater. Today Energy 4 (2017) 34.

[17] T.K.A. Hoang, T.N.L. Doan, J.H. Cho, J.Y.J. Su, C. Lee, C.Y. Lu, P. Chen, Sustainable gel electrolyte containing pyrazole as corrosion inhibitor and dendrite suppressor for aqueous Zn/$LiMn_2O_4$ battery, ChemSusChem 10 (2017) 2816.

[18] X.L. Ji, S. Evers, R. Black, L.F. Nazar, Stabilizing lithium–sulphur cathodes using polysulphide reservoirs, Nat. Commun. 2 (2011) 325.

[19] S. Evers, L.F. Nazar, New approaches for high energy density lithium–sulfur battery cathodes, Accounts Chem. Res. 46 (2013) 1135.

[20] M. Kim, S.-H. Kang, J. Manuel, X.H. Zhao, K.K. Cho, J.H. Ahn, Investigation into the role of silica in lithium polysulfide adsorption for lithium sulfur battery, Mater. Res. Bull. 69 (2015) 29.

[21] G.J. Xu, Z.H. Liu, C.J. Zhang, G.L. Cui, L.Q. Chen, Strategies for improving the cyclability and thermo-stability of $LiMn_2O_4$-based batteries at elevated temperatures, J. Mater. Chem. A 3 (2015) 4092.

[22] A. Konarov, D. Gosselink, Y.G. Zhang, Y. Tian, D. Askhatova, P. Chen, Self-discharge of rechargeable hybrid aqueous battery, ECS Electrochem. Lett. 4 (2015) A151.

[23] H. Yang, R. Xu, X.M. Xue, F.T. Li, G.T. Li, Hybrid surfactant-templated mesoporous silica formed in ethanol and its application for heavy metal removal, J. Hazard. Mater. 152 (2008) 690.

[24] H. Zou, S.S. Wu, J. Shen, Polymer/silica nanocomposites: preparation, characterization, properties, and applications, Chem. Rev. 108 (2008) 3893.

[25] Y.N. Qu, Y.M. Tian, B. Zou, J. Zhang, Y.H. Zheng, L.L. Wang, Y. Li, C.G. Rong, Z.C. Wang, A novel mesoporous lignin/silica hybrid from rice husk produced by a sol–gel method, Bioresource Technol. 101 (2010) 8402.

[26] W.L. Xiong, D.J. Yang, R.S. Zhong, Y. Li, H.F. Zhou, X.Q. Qiu, Preparation of lignin-based silica composite submicron particles from alkali lignin and sodium silicate in aqueous solution using a direct precipitation method, Ind. Crops Prod. 74 (2015) 285.

[27] W.L. Xiong, X.Q. Qiu, D.J. Yang, R.S. Zhong, Y. Qian, Y.Y. Li, H. Wang, A

simple one-pot method to prepare UV-absorbent lignin/silica hybrids based on alkali lignin from pulping black liquor and sodium metasilicate, Chem. Eng. J. 326 (2017) 803.

[28] A.J. Ragauskas, G.T. Beckham, M.J. Biddy, R. Chandra, F. Chen, M.F. Davis, B.H. Davison, R.A. Dixon, P. Gilna, M. Keller, P. Langan, A.K. Naskar, J.N. Saddler, T.J. Tschaplinski, G.A. Tuskan, C.E. Wyman, Lignin valorization: improving lignin processing in the biorefinery, Science 344 (2014) 1246843.

[29] T. Aro, P. Fatehi, Production and application of lignosulfonates and sulfonated lignin, ChemSusChem 10 (2017) 1861.

[30] Y. Qian, Y.H. Deng, X.Q. Qiu, H. Li, D.J. Yang, Formation of uniform colloidal spheres from lignin, a renewable resource recovered from pulping spent liquor, Green Chem. 16 (2014) 2156.

[31] S.S. Nair, S. Sharma, Y.Q. Pu, Q.N. Sun, S.B. Pan, J.Y. Zhu, Y.L. Deng, A.J. Ragauskas, High shear homogenization of lignin to nanolignin and thermal stability of nanolignin-polyvinyl alcohol blends, ChemSusChem 7 (2014) 3513.

[32] Y.Y. Li, X.Q. Qiu, Y. Qian, W.L. Xiong, D.J. Yang, pH-responsive lignin-based complex micelles: preparation, characterization and application in oral drug delivery, Chem. Eng. J. 327 (2017) 1176.

[33] Y. Qian, X.Q. Qiu, X.W. Zhong, D.L. Zhang, Y.H. Deng, D.J. Yang, S.P. Zhu, Lignin reverse micelles for UV-absorbing and high mechanical performance thermoplastics, Ind. Eng. Chem. Res. 54 (2015) 12025.

[34] Y. Qian, X.Q. Qiu, S.P. Zhu, Lignin: a nature-inspired sun blocker for

broad-spectrum sunscreens, Green Chem. 17 (2015) 320.

[35] Y. Qian, X.Q. Qiu, S.P. Zhu, Sunscreen performance of lignin from different technical resources and their general synergistic effect with synthetic sunscreens, ACS Sustainable Chem. Eng. 4 (2016) 4029.

[36] Ł. Klapiszewski, M. Nowacka, G. Milczarek, T. Jesionowski, Physicochemical and electrokinetic properties of silica/lignin biocomposites, Carbohyd. Polym. 94 (2013) 345.

[37] T. Jesionowski, Ł. Klapiszewski, G. Milczarek, Structural and electrochemical properties of multifunctional silica/lignin materials, Mater. Chem. Phys. 147 (2014) 1049.

[38] Ł. Klapiszewski, P. Bartczak, M. Wysokowski, M. Jankowska, K. Kabat, T. Jesionowski, Silica conjugated with kraft lignin and its use as a novel ‘green’ sorbent for hazardous metal ions removal, Chem. Eng. J. 260 (2015) 684.

[39] Ł. Klapiszewski, T. Rzemieniecki, M. Krawczyk, D. Malina, M. Norman, J. Zdarta, I. Majchrzak, A. Dobrowolska, K. Czaczyk, T. Jesionowski, Kraft lignin/silica–AgNPs as a functional material with antibacterial activity, Colloids Surfaces B 134 (2015) 220.

[40] P.C. Lian, X.F. Zhu, H.F. Xiang, Z. Li, W.S. Yang, H.H. Wang, Enhanced cycling performance of Fe_3O_4–graphene nanocomposite as an anode material for lithium-ion batteries, Electrochim. Acta 56 (2010) 834.

[41] P.C. Lian, X.F. Zhu, S.Z. Liang, Z. Li, W.S. Yang, H.H. Wang, High reversible capacity of SnO_2/graphene nanocomposite as an anode material for lithium-ion

batteries, Electrochim. Acta 56 (2011) 4532.

[42] Y.J. Mai, X.L. Wang, J.Y. Xiang, Y.Q. Qiao, D. Zhang, C.D. Gu, J.P. Tu, CuO/graphene composite as anode materials for lithium-ion batteries, Electrochim. Acta 56 (2011) 2306.

[43] G.H. Yuan, J.T. Bai, T.N.L. Doan, P. Chen, Synthesis and electrochemical properties of $LiFePO_4$/graphene composite as a novel cathode material for rechargeable hybrid aqueous battery, Mater. Lett. 158 (2015) 248.

[44] J. Zhi, A.Z. Yazdi, G. Valappil, J. Haime, P. Chen, Artificial solid electrolyte interphase for aqueous lithium energy storage systems, Sci. Adv. 3 (2017) e1701010.

[45] S. Brunaue, P.H. Emmett, E. Telle, Adsorption of gases in multimolecular layers, J. Am. Chem. Soc. 60 (1938) 309.

[46] F. Lu, S.-H. Wu, Y. Hung, C.-Y. Mou, Size effect on cell uptake in well-suspended, uniform mesoporous silica nanoparticles, Small 5 (2009) 1408.

[47] Yu.M. Chernoberezhskii, A.A. Atanesyan, A.B. Dyagileva, A.V. Lorentsson, T.V. Leshchenko, Effect of the concentration of sulfate lignin on the aggregation stability of its aqueous dispersions, Colloid J. 64 (2002) 637.

[48] X.Q. Qiu, Q. Kong, M.S. Zhou, D.J. Yang, Aggregation behavior of sodium lignosulfonate in water solution, J. Phys. Chem. B 114 (2010) 15857.

[49] M.F. Yan, D.J. Yang, Y.H. Deng, P. Chen, H.F. Zhou, X.Q. Qiu, Influence of pH on the behavior of lignosulfonate macromolecules in aqueous solution, Colloids Surf. A: Physicochem. Eng. Aspects 371 (2010) 50.

[50] T.K.A. Hoang, T.N.L. Doan, K.E.K. Sun, P. Chen, Corrosion chemistry and protection of zinc & zinc alloys by polymer-containing materials for potential use in rechargeable aqueous batteries, RSC Adv. 5 (2015) 41677.

Figure Captions

Fig. 1. (a) N_2 adsorption–desorption isotherms of the LSCs. (b) Pore volume curves of the LSCs.

Fig. 2. TEM images of the LSC-1 and LSC-2.

Fig. 3. Rate performance of the batteries using LSC-1, G, and LSC-1+G based cathode, respectively.

Fig. 4. Cyclability of the batteries at 1 C rate with CC−CV charging and CC discharging mode.

Fig. 5. OCV vs time profiles of batteries using reference cathode, cathode containing LSC-1, G, and LSC-1+G, respectively.

Fig. 6. PEIS of different cathodes in the three electrode system and their corresponding fitting results.

Table 1

Float charge performance of the batteries using LSC based cathode.

Sample	Dosage (m_{sample}/m_{LMO})	Discharge capacity at 0.2 C ($mAh \cdot g^{-1}$)	Float charge capacity at 0.2 C ($mAh \cdot g^{-1}$)
Reference	--	119.1 ± 1.0	14.3 ± 1.6
LSC-1	2 wt %	110.1 ± 1.2	6.1 ± 0.6
LSC-2	2 wt %	119.8 ± 2.9	10.1 ± 1.3
LSC-3	2 wt %	109.9 ± 3.7	18.0 ± 0.9

Table 2

Float charge performance of the batteries using LSC, G and LSC+G based cathode.

Sample	Dosage (m_{sample}/m_{LMO})	Discharge capacity at 0.2 C ($mAh \cdot g^{-1}$)	Float charge capacity at 0.2 C ($mAh \cdot g^{-1}$)
Reference	--	119.1 ± 1.0	14.3 ± 1.6
LSC-1	2 wt %	110.1 ± 1.2	6.1 ± 0.6
G	2 wt %	122.1 ± 1.5	9.9 ± 1.5
LSC-1+G (1:1)	2 wt %	115.5 ± 1.9	7.9 ± 2.5
LSC-1+G (1:1)	3 wt %	122.1 ± 0.5	7.2 ± 0.2
LSC-1+G (1:1)	4 wt %	124.7 ± 0.6	12.4 ± 1.2
LSC-1+G (1.5:1)	4 wt %	125.6 ± 1.5	10.8 ± 1.8
LSC-1+G (2:1)	4 wt %	116.6 ± 3.4	7.4 ± 2.3

Table 3

Parameters from the fitting results of PEIS by using ZView.

Cathode	Ohmic resistance (R_S, Ω)	Charge-transfer resistance (R_1, Ω)	Li^+ diffusivity (D_{Li}, $cm^2 \cdot s^{-1}$)
Reference	2.158	43.25	4.753×10^{-11}
LSC-1 (2 wt%)	2.248	43.64	3.731×10^{-11}
G (2 wt%)	2.111	23.13	8.318×10^{-11}
LSC-1+G (3 wt%)	2.142	38.49	4.868×10^{-11}

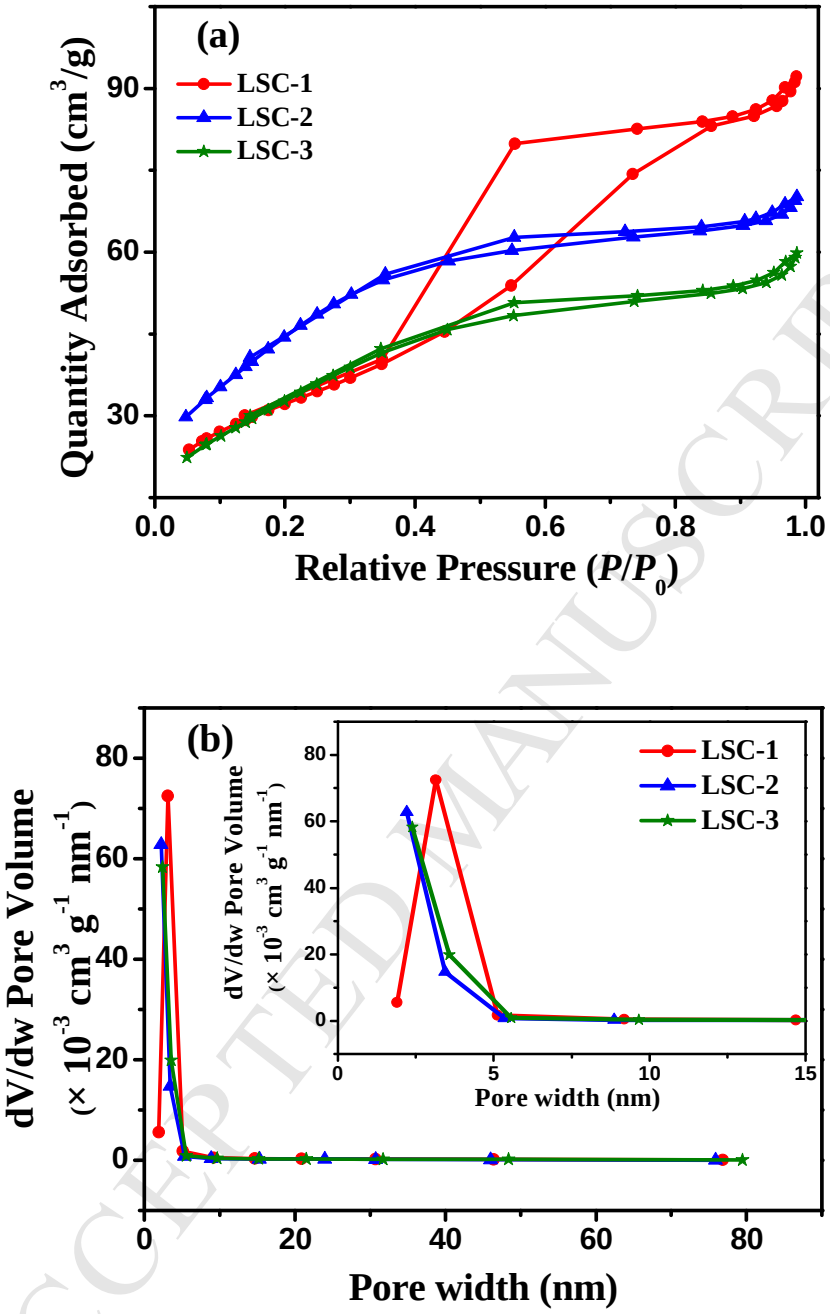

Fig. 1. (a) N_2 adsorption–desorption isotherms of the LSCs. (b) Pore volume curves of the LSCs.

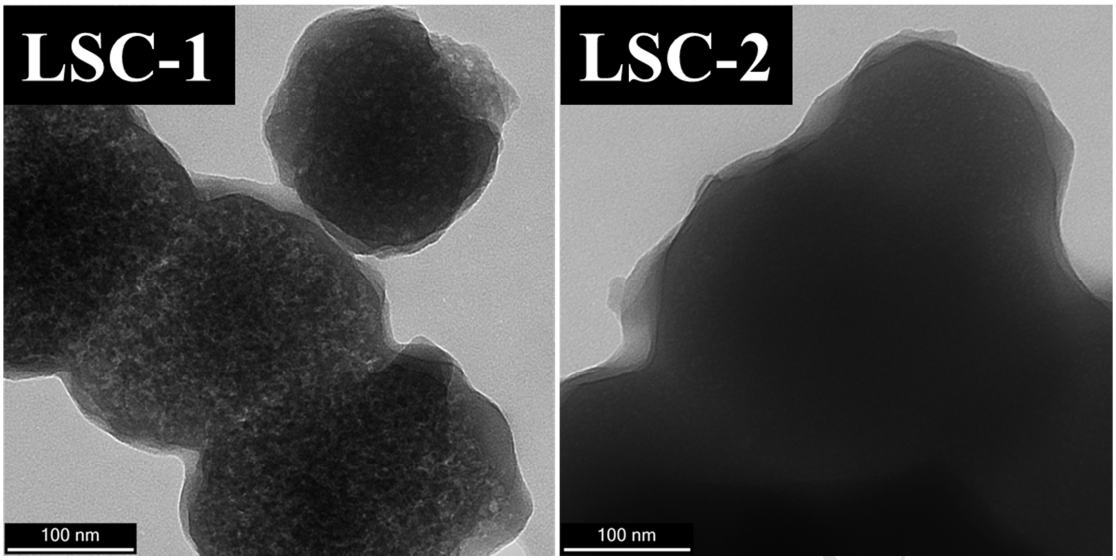

Fig. 2. TEM images of the LSC-1 and LSC-2.

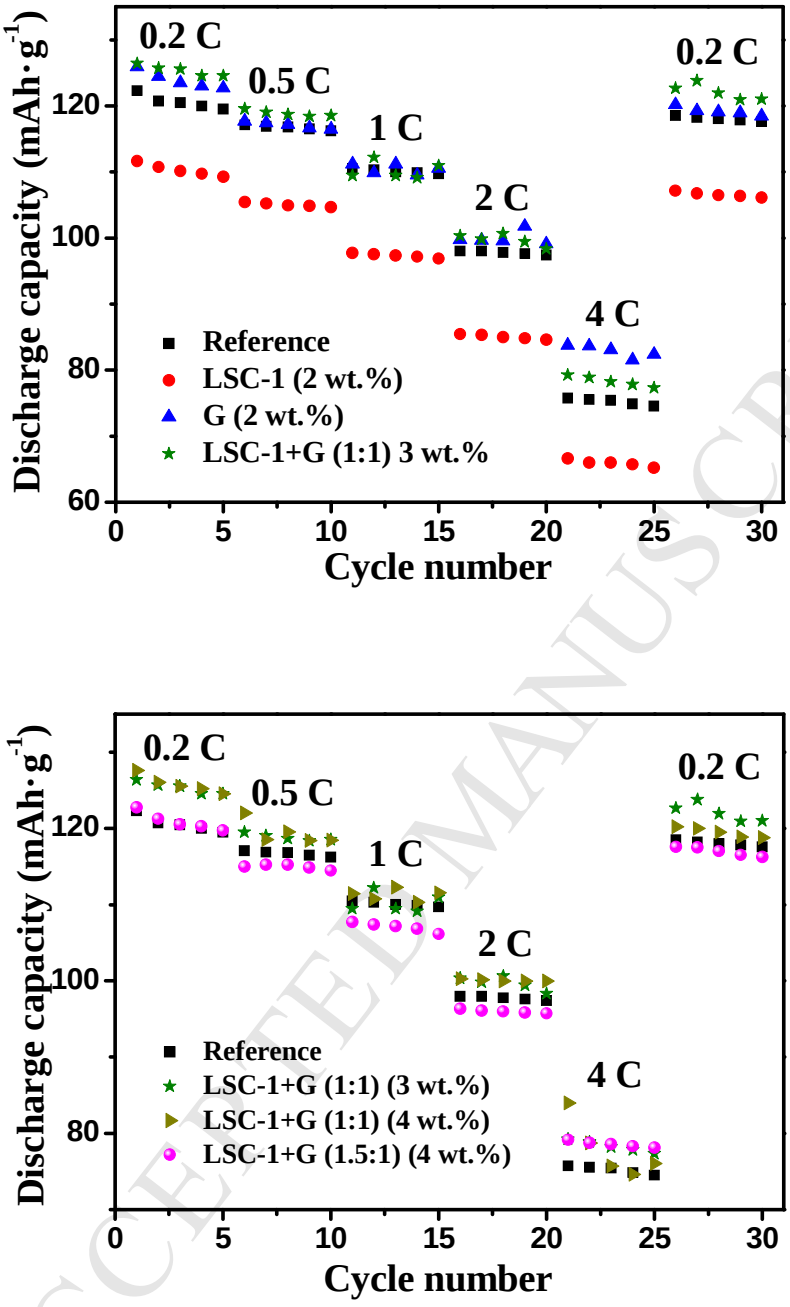

Fig. 3. Rate performance of the batteries using LSC-1, G, and LSC-1+G based cathode, respectively.

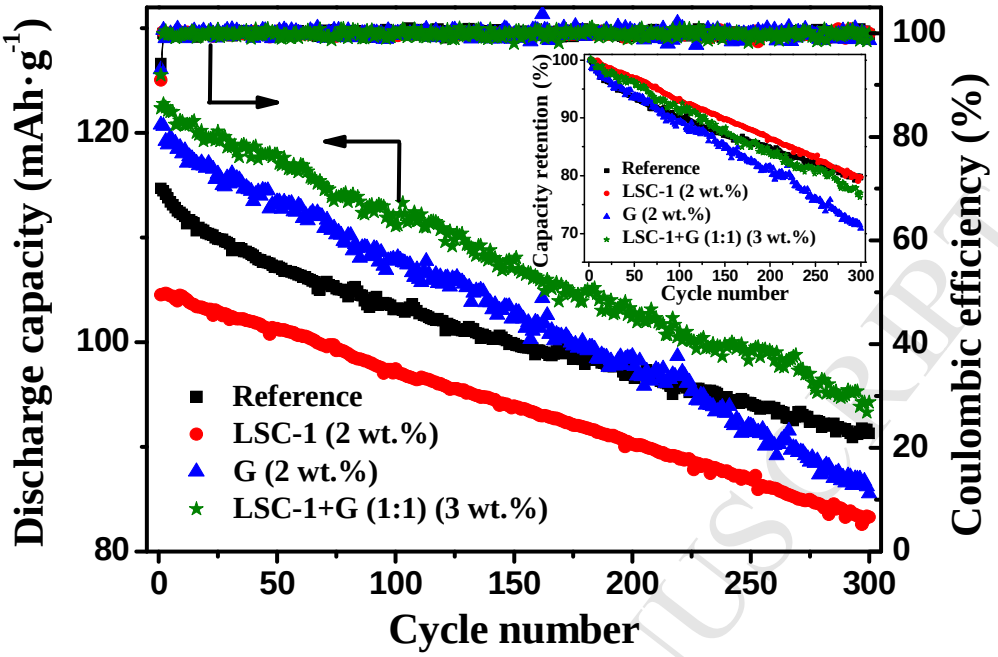

Fig. 4. Cyclability of the batteries at 1 C rate with CC−CV charging and CC discharging mode.

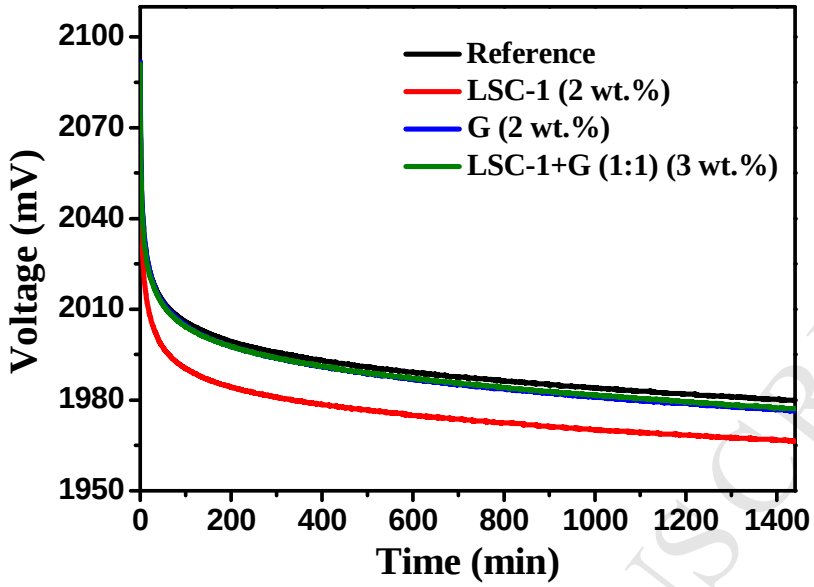

Fig. 5. OCV vs time profiles of batteries using reference cathode, cathode containing LSC-1, G, and LSC-1+G, respectively.

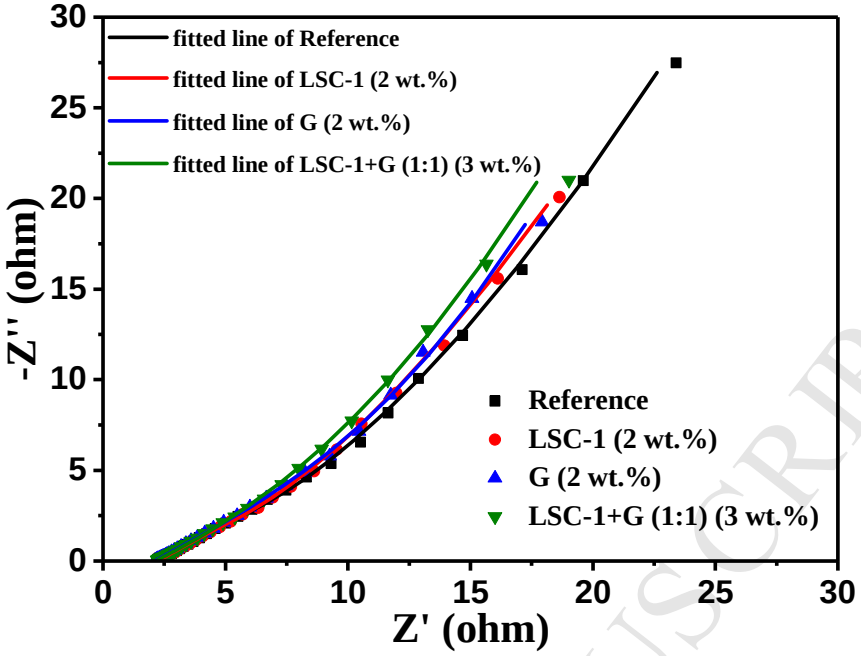

Fig. 6. PEIS of different cathodes in the three electrode system and their corresponding fitting results.